PAPER • OPEN ACCESS

A lionfish-inspired predation strategy in planar structured environments*

To cite this article: Anthony A Thompson *et al* 2023 *Bioinspir. Biomim.* **18** 046022

IOP Publishing Bioinspir. Biomim. 18 (2023) 046022 https://doi.org/10.1088/1748-3190/ace016

Bioinspiration & Biomimetics

OPEN ACCESS

RECEIVED
23 January 2023

REVISED
5 June 2023

ACCEPTED FOR PUBLICATION
20 June 2023

PUBLISHED
30 June 2023

PAPER

A lionfish-inspired predation strategy in planar structured environments*

Anthony A Thompson[1,**], Ashley N Peterson[2], Matthew J McHenry[2] and Derek A Paley[3]

[1] Department of Aerospace Engineering, University of Maryland, College Park, MD 20742, United States of America
[2] Department of Ecology and Evolutionary Biology, University of California, Irvine, Irvine, CA 92697, United States of America
[3] Department of Aerospace Engineering and the Institute for Systems Research, University of Maryland, College Park, MD 20742, United States of America
* This work was supported by ONR Grant No. 115239289.
** Author to whom any correspondence should be addressed.

E-mail: athomp95@umd.edu

Keywords: pursuit and evasion, structured environments, game theory, lionfish pursuit, stochastic evasion

Supplementary material for this article is available online

Abstract

This paper investigates a pursuit-evasion game with a single pursuer and evader in a bounded environment, inspired by observations of predation attempts by lionfish (*Pterois sp.*). The pursuer tracks the evader with a pure pursuit strategy while using an additional bioinspired tactic to trap the evader, i.e. minimize the evader's escape routes. Specifically, the pursuer employs symmetric appendages inspired by the large pectoral fins of lionfish, but this expansion increases its drag and therefore its work to capture the evader. The evader employs a bioinspired randomly-directed escape strategy to avoid capture and collisions with the boundary. Here we investigate the trade-off between minimizing the work to capture the evader and minimizing the evader's escape routes. By using the pursuer's expected work to capture as a cost function, we determine when the pursuer should expand its appendages as a function of the relative distance to the evader and the evader's proximity to the boundary. Visualizing the pursuer's expected work to capture everywhere in the bounded domain, yields additional insights about optimal pursuit trajectories and illustrates the role of the boundary in predator-prey interactions.

1. Introduction

Interactions between predators and their prey have fascinated a variety of scientific disciplines for several decades. For biologists, predator-prey interactions inform the structure of ecosystems [1–3] and characterize the pursuit and evasive behaviors of predators and prey [1, 4–13]. Engineers and mathematicians use these interactions to develop dynamic and kinematic models for missile guidance [14] and differential games [15, 16] and to derive pursuit and evasion strategies for robotic systems [17–24].

For example, lionfish (*Pterois sp.*) will actively pursue maneuverable prey fishes with a pure pursuit targeting strategy, often approaching their prey slowly to avoid inducing a startle response [3, 5, 10]. In addition, lionfish have large fan-like pectoral fins (depicted in figures 1(a) and (b)) that may serve to restrict prey movement [7, 8]. The purpose of using the lionfish's pectoral fins during predation is not well studied, but the observations in [7, 8] briefly mention this behavior and hypothesize that the lionfish use their fins to herd prey to confined areas like coral reefs.

Expanding the pectoral fins may increase the lionfish's perceived size and studies have shown that the perceived larger size of predators can initiate a prey's flee response quicker than a smaller predator [25, 26]. The large surface area of the pectoral fins are also likely drag inducing, yet lionfish rarely pursue a prey without expanding them. After examining the observations in [6–8], we hypothesize that there is a trade-off between expanding the pectoral fins to trap prey and retracting the fins to minimize hydrodynamic drag. We seek to understand the trade-off between these two strategies and we seek to understand the role a boundary plays in predator-prey interactions. To answer the questions of when and why a predator

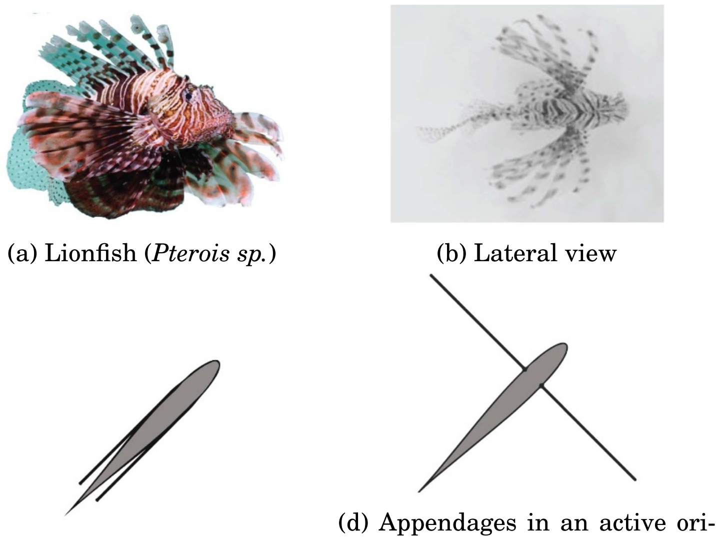

(a) Lionfish (*Pterois sp.*)

(b) Lateral view

(c) Model of pursuer

(d) Appendages in an active orientation

Figure 1. Lionfish (*Pterois sp.*) serve as bioinspiration for a shape-changing predator. (a) Lateral view of a lionfish (*Pterois miles*); (b) dorsal view of a lionfish (*Pterois volitans*; in black and white); (c) depicts the model of the pursuer with appendages in the resting orientation; and (d) the pursuer's appendages are in an active orientation.

should prioritize trapping prey over minimizing its drag during predation in a bounded setting, we derive a pursuit-evasion game in a bounded environment with a single pursuer with symmetric appendages and a single evader.

Pursuit-evader games attempt to derive optimal pursuit strategies by modeling both agents as particles. These particle models are often based on kinematic modeling [14] and used in theoretical differential games [15]. In [14], Shneydor derives kinematic models for missile guidance for a variety of pursuit strategies like classical pursuit (also known as pure pursuit), deviated pure pursuit, and parallel navigation (also known as motion camouflage). Differential games consider the kinematics of both agents and study how their pursuit and evasion strategies affect the outcome of the interaction. For zero-sum differential games, the pursuer seeks to minimize some cost function and the evader seeks to maximize it such that the total sum of their costs is zero [15]. The work presented here adopts the pure pursuit kinematic models from [14] and applies them in a novel zero-sum pursuit-evasion game.

A common assumption of kinematic pursuit models is that the pursuer is faster than the evader, which guarantees capture [14, 17, 21]. However, capture of a faster evader is possible for a slower pursuer by using the Appollonius circle pursuit method. In the Apollonius circle method, a slow pursuer computes reachable positions that intersects the non-maneuvering evader's trajectory. The points of intersection between the pursuit and evasion trajectories lie on the Appollonius circle which contain positions where the pursuer and evader are projected coincide. The circle's center and radius correspond to the positions where capture is guaranteed [20, 24, 27]. The method of Appollonius circle assumes pursuit of a faster non-maneuvering evader, whereas [14] assumes the evader is non-maneuvering and is slower than the pursuer. These mathematical frameworks give insight about pursuit trajectories and provide conditions on both the pursuer and the evader for successful capture. When these conditions are satisfied, the time required to capture the evader can be determined. In the present work, the time to capture is used to compute the work required to capture the evader, which is maneuvering to avoid the predator.

The unique ability of animals to alter their behavior, locomotion, and morphology in response to a stimuli inspires and informs both biologists and engineers. Fishes are widely studied by engineers interested in developing control systems and autonomous underwater vehicles. Bioinspiration also plays an integral role in pursuit-evasion games [16, 17] and pursuit-evasion models have previously been applied to a handful of fish species [4, 9, 10, 13, 21]. For the present game, the pursuer is modeled as a rigid streamlined body with symmetric appendages in pure pursuit of the evader. In the resting orientation, the pursuer's appendages are held against the body, parallel to the pursuer's sagittal plane as in figure 1(c), whereas in the active orientation the appendages are expanded perpendicular to the sagittal plane as in figure 1(d). The pursuer uses its appendages in an effort to trap the evader, i.e. minimize the evader's escape routes by blocking its view of possible flee directions, but this appendage orientation increases the pursuer's surface area and therefore its hydrodynamic drag.

In biological systems, animal prey may employ an optimal evasion strategy (classical evasion), where the evader attempts to maximize the relative distance to the pursuer [10, 13, 28], or a protean strategy, where the evader senses the relative position of the pursuer and flees in a random direction to be less predictable [10–12, 29]. Observations of an evader's escape direction yields a probability density function that is used for mathematical predictions [12]. The movement patterns of animals also play a role in the pursuit-evasion interaction. Mathematical models often assume constant locomotion, however, a variety of aquatic, aerial, and terrestrial species use intermittent locomotion [30, 31]. For many fishes, intermittent locomotion is split into two discrete phases that correspond to acceleration and deceleration. During the acceleration phase the fish will generate thrust and actively steer itself, whereas during the deceleration phase the fish glides through the water without active steering [4, 32]. Inspired by observations of intermittent prey [5, 6], the evader in the present study uses an intermittent-steering kinematic model (with a constant speed) and a protean strategy to evade the pursuer and to avoid collisions with the boundary. The evader's random flee direction has a probability density function that is affected by the evader's proximity to the walls of the environment, the proximity to the pursuer, and the pursuer's appendage orientation.

We introduce a pursuit-evasion game with a single pursuer and a single evader moving at a constant speed in a still fluid. We aim to study the trade-off between the pursuer using its appendages to minimize its hydrodynamic drag and minimize the evader's escape routes. In an effort to study the effects of a bounded environment on predation, the game occurs in a planar convex environment. The convex assumption provides geometric conditions that simplify the environment while maintaining its role in pursuit-evasion interactions. Using the expected work required to capture the evader as an objective function, we show that minimizing the evader's escape routes can outweigh the effect of incurring additional drag. With this metric, we determine the regions in the bounded environment where it is advantageous for the pursuer to expand its appendages in the active orientation. Similarly, we show that the presence of a boundary positively affects the pursuer by expanding the size of the active orientation shape-changing region.

The contributions of this paper are as follows: (1) a pursuer-evader interaction model with a shape-changing pursuer and an intermittently-steering evader; (2) a mathematical model for the probability density of the evader's escape heading in a bounded environment; (3) a metric to determine when the pursuer should change shape to minimize the evader's escape routes; and (4) a qualitative assessment of the optimal pursuit trajectories as a function of the evader's position in a bounded environment. These results provide a framework for a new bioinspired pursuit-evasion interaction, give insight into the predation behaviors found in nature, and give a fundamental understanding of how a bounded environment influences predation strategies.

This paper is organized as follows. Section 2 provides mathematical and physical preliminaries, including an overview of the complex numbers and random variables used for analysis, and pursuit and evasion strategies. Section 3 formulates the problem, equations of motion, the evader's avoidance and escape regions, and the evader's escape heading probability density function. Section 4 presents the expected work required to capture the evader, discusses when the pursuer should prioritize trapping the evader over minimizing the work to capture, and provides a qualitative assessment of the optimal pursuit trajectories. Section 5 summarizes the results and describes ongoing and future work.

2. Background

This section reviews complex numbers, random variables, and the kinematics of classical pursuit and the protean evasion strategy.

2.1. Complex variables

To reduce the number of equations, this paper uses complex numbers to express the position and orientation of the pursuer and the evader. A complex number has real and imaginary components and can be expressed as $h = x + jy$. The imaginary component of h is multiplied by the imaginary unit j such that $\mathrm{Im}(h) = y$, and the real component of h is $\mathrm{Re}(h) = x$. Since complex numbers have two components, they can be visualized in a two-dimensional space called the complex plane $\mathbb{C}$.

A common tool for dimension reduction is to express vectors with two orthogonal components as a complex number. Let the horizontal and vertical components of vector $\boldsymbol{v}$ be $\boldsymbol{v} = [x, y]$, where the bold notation represents a vector. By aligning the horizontal direction with the real axis and the vertical direction with the imaginary axis, we can express vector $\boldsymbol{v}$ as a complex number $v = x + jy$.

Similarly, the orientation of a vector $\boldsymbol{v}$ can be expressed as the phase θ of a complex number v, where

$$\theta = \arg(v). \tag{1}$$

The arg() operator is the argument of the complex number. Likewise, the magnitude of a complex number is determined by taking its absolute value.

Using the phase θ and magnitude $|v|$ of v, we can express the position of a particle in complex polar form with Euler's formula [33], such that

$$v = |v|e^{j\theta} = |v|(\cos\theta + j\sin\theta). \tag{2}$$

In general, since the imaginary component is orthogonal to the real component of a complex number, multiplying that number by j rotates its phase by $\pi/2$ radians in the counter-clockwise direction.

2.2. Expected value of a random variable

To analyze the stochastic nature of a random variable, we use tools from probability theory. Let $\mathcal{X}$ be a random variable on the real number line. The probability density function $f(\mathcal{X})$ is the likelihood of $\mathcal{X}$ being within a certain range of values. The expected value of $\mathcal{X}$ is [34]

$$E[\mathcal{X}] = \int_{-\infty}^{\infty} \mathcal{X} f(\mathcal{X}) d\mathcal{X}. \tag{3}$$

If random variable $\mathcal{X}$ is used in a function $Y = h(\mathcal{X})$ with probability density function $f(\mathcal{X})$, then the expected value of the function is [34]

$$E[Y] = \int_{-\infty}^{\infty} h(\mathcal{X}) f(\mathcal{X}) d\mathcal{X}. \tag{4}$$

We adapt (4) to compute the expected work required for the pursuer to capture an evader using the protean evasion strategy in section 4.

2.3. Pursuit and evasion strategies

Pursuit and evasion are well-studied topics with applications in missile guidance [14], biological predation [9, 10, 21], and engineered systems [17, 20, 22, 23]. Pure pursuit [14] is characterized by having a pursuer P heading directly towards an evader E along their line-of-sight vector, i.e. the vector from P to E.

Let the pursuer's position be $r_P = x_P + jy_P \in \mathbb{C}$. Let θ_P and V_P be the pursuer's velocity orientation and speed, respectively. Similarly, let r_E, θ_E, and V_E be the evader's position, heading, and speed, respectively. The line-of-sight vector is

$$r_{E/P} = r_E - r_P \tag{5}$$

and the orientation of the line-of-sight vector is

$$\alpha = \arg(r_{E/P}), \tag{6}$$

as shown in figure 2.

Common assumptions in the pursuit literature are that both pursuer and evader have constant speeds and that the pursuer has a higher speed than the evader [14, 15]. The ratio of the two speeds is $K = V_P/V_E$. In the present model, the pursuer's speed is arbitrarily set to $V_P = 1.05$ m s^{-1} and the evader's speed is $V_E = 1$ m s^{-1} such that $K = 1.05$.

In pure pursuit, the time required to capture a non-maneuvering evader is [14]

$$\Delta t = \frac{|r_{E/P}|}{V_E} \frac{K + \cos(\alpha - \theta_E)}{K^2 - 1}. \tag{7}$$

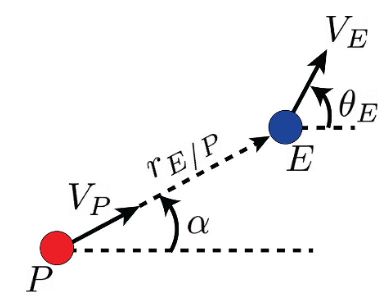

Figure 2. Pure pursuit model using particle kinematics.

Note that (7) is only valid for $K > 1$, i.e. when the pursuer is strictly faster than the evader.

The line-of-sight orientation (6) is used as the reference heading for the pursuer in section 3 and (7) is used to compute the work required to capture the evader in section 4.

An evasion strategy observed in animals is the protean strategy [10, 11], where the evader senses the pursuer and flees in a random escape direction θ_d. The stochastic nature of this evasion strategy makes the evader less predictable to the pursuer. The random escape direction has a probability density function that depends on the evader's proximity to the boundary and relative distance to the pursuer. The probability density function of θ_d is derived in section 3 and used to compute the expected value of the work required to capture the evader in section 4.

To compute the work executed during pursuit, let T_P be the pursuer's thrust, which we assume is aligned with its velocity. Assuming the pursuer has constant speed, the work performed by T_P depends on the path the pursuer takes from time t_0 to $t_0 + \Delta t$, where Δt is given by (7), such that [35]

$$W_P = \int_{t_0}^{t_0+\Delta t} T_P V_P \mathrm{d}t. \tag{8}$$

To find the work required to capture the evader, substitute (7) into (8) and evaluate the integral, i.e.

$$W_P = T_P |r_{E/P}| \frac{K^2 + K\cos(\alpha - \theta_E)}{K^2 - 1}. \tag{9}$$

Note that the work required for the pursuer to capture the evader depends on the evader's heading θ_E.

The randomness of the evader's protean evasion strategy makes the work in (9) a stochastic process and we use tools from probability theory to analyze the expected value of work, also called the expected work. In section 4, (9) is adapted to analyze the work required to capture the evader.

3. Problem formulation

This paper considers a pursuit-evasion game with a single pursuer P and evader E in a planar convex environment. The pursuer is modeled as a streamlined rigid body with symmetric movable appendages and its objective is to capture the evader using pure pursuit. The evader is modeled as a self-propelled particle and employs the protean strategy in an effort to avoid capture. Capture is defined as the coincidence of the frontmost point on the pursuer's body and evader.

During pursuit, the pursuer orients its appendages to minimize the evader's escape directions; however, expanding the appendages increases drag. We explore the trade-off between minimizing the work to capture the evader and minimizing the evader's escape directions by using the expected work to capture as the cost function.

The following subsections present the planar interaction model between a pursuer P and an evader E in a bounded environment. First, we derive the equations of motion for the pursuer and evader. Second, we introduce the evader's avoidance and escape regions that are used to derive the probability density function of the evader's escape heading. Third, we derive the probability density function for the evader's escape heading.

3.1. Equations of motion

Let the pursuer's body length, width, and appendage length be l_P, w_P, and l_f, respectively. The pursuer's center of mass is positioned at $r_P = x_P + jy_P$ and the body's frontmost point is

$$r_{Pf} = r_P + \frac{l_P}{4} e^{j\theta_P}, \tag{10}$$

where θ_P is the pursuer's heading.

Inspired by the predation strategies of lionfish [1, 7, 10], the pursuer uses its appendages to minimize the evader's escape routes, but doing so affects the pursuer's size and surface area. Let ψ be the appendage orientation with respect to θ_P. Since the appendages are symmetric, ψ is the orientation of the right appendage and $-\psi$ is the orientation of the left appendage. The endpoints of the left and right appendages are positioned at r_{AL} and r_{AR}, respectively, where

$$r_{AL} = r_P + \frac{1}{2} w_P j e^{j\theta_P} + l_f e^{j(\theta_P - \psi)} \tag{11}$$

$$r_{AR} = r_P - \frac{1}{2} w_P j e^{j\theta_P} + l_f e^{j(\theta_P + \psi)}. \tag{12}$$

When $\psi = 0$, the appendages are held parallel to the line-of-sight vector and the pursuer is in its narrowest configuration, and when $\psi = \pi/2$, the appendages are perpendicular to the line-of-sight vector and the pursuer is in its widest configuration. For simplicity, let ψ be treated as a switching parameter with values of either $\psi = 0$ or $\psi = \pi/2$. Increasing the frontal area of the pursuer comes at the cost of additional drag, modeled as

$$D_p = b\left(1 + H\sin(\psi)\right) V_P, \tag{13}$$

where $b > 0$ is the nominal drag coefficient and $H > 0$ is the percent drag increase due to the orientation of the appendages. We use (13) in section 4 to compute the work and expected work to capture the evader as a function of ψ.

To model the planar locomotion of the pursuer, we model a thrust force T_P, linear drag force D_P, and turning rate u_P. u_P directly controls rate of change of the the pursuer's direction of motion. The body is aligned with this direction. We also assume that the pursuer has a constant speed V_P, i.e. the thrust and drag forces cancel. The equations of motion of P are

$$\dot{r}_P = V_P e^{j\theta_P} \tag{14}$$

$$\dot{\theta}_P = u_P. \tag{15}$$

Using the pure pursuit strategy, the pursuer seeks to align its heading with the line-of-sight vector such that

$$u_P = K_P \sin(\alpha - \theta_P), \tag{16}$$

where α is (6) and $K_P > 0$ is a steering control gain.

The evader, on the other hand, is modeled as a point mass self-propelled particle E with intermittent steering. The intermittent steering is divided into an active steering phase during which the evader changes its heading over a duration of β seconds and a non-steering phase during which the evader has a constant heading over a duration of $\mathcal{T}$ seconds. Let the evader's constant speed be denoted as V_E and its heading be θ_E. Adapting the planar intermittent locomotion model from [36], the equations of motion of E are shown in figure 3. We assume β is much smaller than $\mathcal{T}$. The completion of a single active steering phase and single non-steering phase is called a cycle, where k is the cycle number [36].

Using the protean evasion strategy, the evader steers towards a random escape heading θ_d during the active steering phase and continues to travel along θ_d during the non-steering phase. Let $u_E = K_E \sin(\theta_d - \theta_E)$ be the steering control input, where $K_E > 0$ is a control gain, and the closed-loop heading dynamics during the active steering phase are $\dot{\theta}_E = K_E \sin(\theta_d - \theta_E)$.

Figure 4 illustrates the pursuer-evader interaction model.

The pursuit and evasion trajectories are governed by the closed-loop dynamics of the pursuer and the evader. Figure 5 illustrates the pursuer's pure pursuit strategy and the evader's protean strategy in a bounded environment shown by solid black lines. In figure 5(a), both the pursuer and evader are in

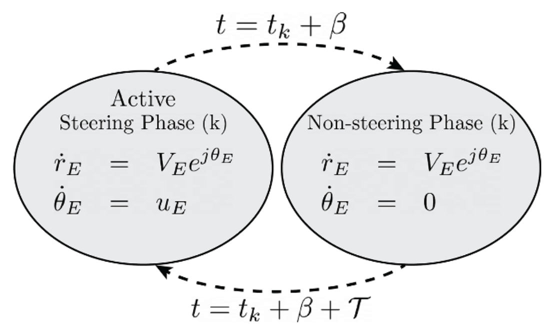

Figure 3. Evader intermittent dynamics split into active steering and non-steering phases. β is the time duration of active steering, $\mathcal{T}$ is the non-steering duration, t is the current time, and t_k is the time when the kth active steering phase started.

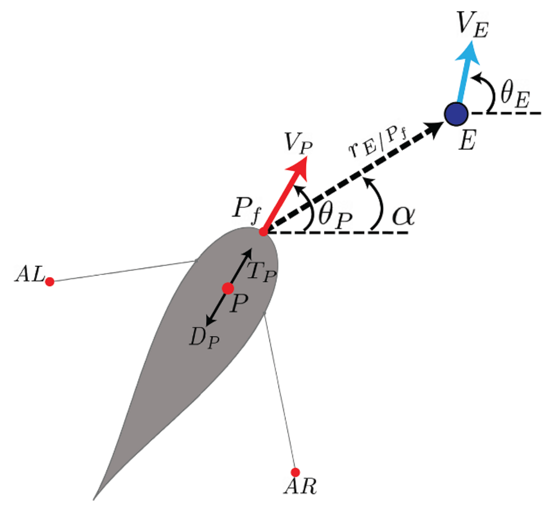

Figure 4. Illustration of the pursuer and the interaction with the evader.

their initial configuration where the pursuer has its appendages retracted and is not sensed by the evader. The evader has a limited sensing range with maximum radius R, here arbitrarily set to 1 m, shown as the lightly shaded blue region in figure 5. Let $\mathcal{R}_{\mathcal{S}} \in \mathbb{R}^2$ be the set of points within the evader's sensing range. If the pursuer or the boundary is outside of $\mathcal{R}_{\mathcal{S}}$, then the evader does not respond to their presence. However, if the pursuer or boundary are inside of $\mathcal{R}_{\mathcal{S}}$, then the evader responds by steering away from them in a random direction θ_d according to its probability density function.

At the start of the simulation, the evader enters its active steering phase during which it randomly selects a desired heading θ_d. The next snapshot in figure 5(b) shows the pursuer entering the evader's sensing region and expanding its appendages. The evader senses the pursuer while in its non-steering phase, so it continues to move in the θ_d direction until the next cycle. In figure 5(c), the evader has entered the next cycle during which a new θ_d is randomly selected to avoid the pursuer by steering in the opposite direction. The pursuer keeps its appendages expanded to minimize the evader's escape routes. Lastly, in figure 5(d), the evader again steers in a random direction to avoid the pursuer, however, the pursuer captures the evader during the non-steering phase. The simulation parameter values for the pursuer and the evader are shown in table 1. The size of the pursuer's body length, body width, and appendage length were adapted from [37].

3.2. The evader's avoidance and escape regions

The goal of the evader is to avoid capture from the pursuer and avoid collisions with the boundary $\mathcal{B} \in \mathbb{R}^2$. Due to the limited sensing range, the evader can only respond to these obstacles when they are in its sensing region $\mathcal{R}_{\mathcal{S}}$.

When the pursuer is within the sensing range, the evader detects its relative direction and size. Let $r_{E/AL}$ and $r_{E/AR}$ be the relative positions of the pursuer's left and right appendages with respect to the evader, respectively, i.e.

$$r_{E/AL}(\psi) = (r_E - r_P) - \frac{1}{2} w_P j e^{j\theta_P} - l_f e^{j(\theta_P - \psi)} \quad (17)$$

$$r_{E/AR}(\psi) = (r_E - r_P) + \frac{1}{2} w_P j e^{j\theta_P} - l_f e^{j(\theta_P + \psi)}. \quad (18)$$

The corresponding relative directions of the left and right appendages are

$$\theta_{AL}(\psi) = \arg(r_{E/AL}(\psi)) \quad (19)$$

$$\theta_{AR}(\psi) = \arg(r_{E/AR}(\psi)), \quad (20)$$

respectively, and the perceived size of the pursuer is the smallest counter-clockwise arc length δ_P between θ_{AL} and θ_{AR} projected onto the evader's maximum sensing radius, i.e.

$$\delta_P(\psi) = R\left(\arg\left(e^{j(\theta_{AL}(\psi) - \theta_{AR}(\psi))}\right)\right). \quad (21)$$

Note that $\delta_P(\psi) \geqslant 0$ is the counter-clockwise arc length and has its maximum value when the appendages are fully expanded.

Similarly, when the boundary is within its sensing range, the evader detects its direction and angular displacement relative the evader's position and heading, respectively. Let $\theta_{\mathcal{B}_i}$ and $\theta_{\mathcal{B}_{i+1}}$ be the angles of the ith intersection between the sensible region and the boundary, and let $\delta_{\mathcal{B}_i} \geqslant 0$ be the smallest counter-clockwise arc length between $\theta_{\mathcal{B}_i}$ and $\theta_{\mathcal{B}_{i+1}}$ projected onto the evader's maximum sensing radius, i.e.

$$\delta_{\mathcal{B}_i} = R\left(\arg\left(e^{j\left(\theta_{\mathcal{B}_i} - \theta_{\mathcal{B}_{i+1}}\right)}\right)\right). \quad (22)$$

To avoid capture, the evader avoids all directions between θ_{AL} and θ_{AR} along arc length δ_P and, to avoid collisions, the evader avoids all directions between $\theta_{\mathcal{B}_i}$ and $\theta_{\mathcal{B}_{i+1}}$ along arc length $\delta_{\mathcal{B}_i}$. We now introduce the

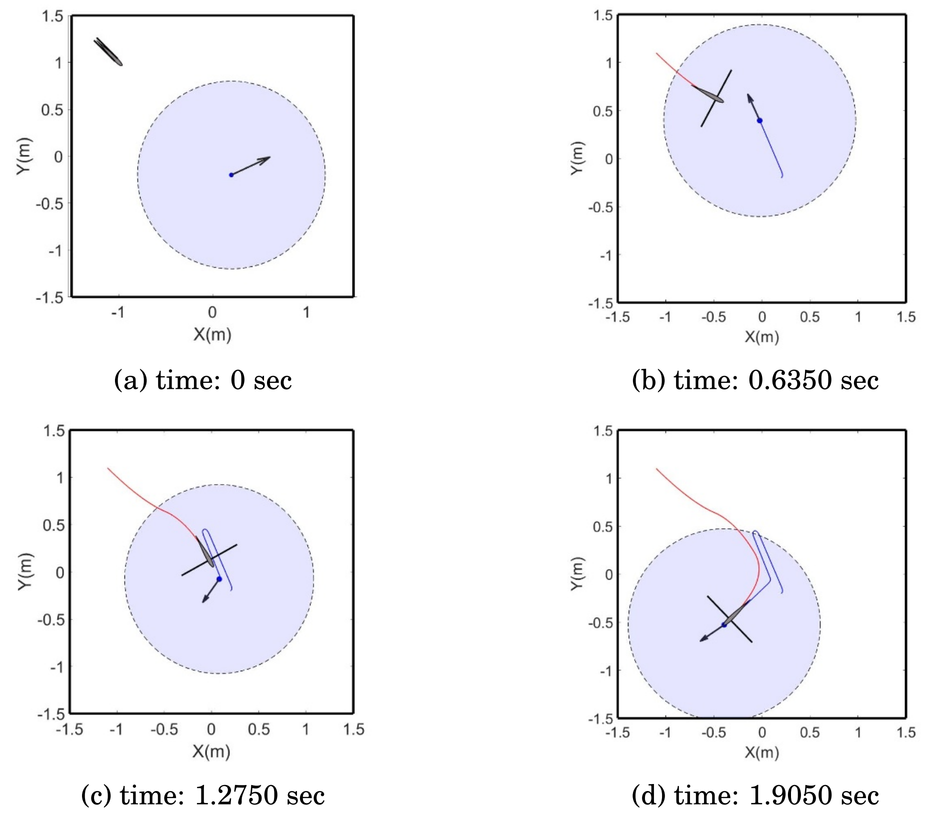

Figure 5. Pure pursuit and protean evasion trajectories in a bounded environment at intervals of 0.6350 s, showing (a) the initial configuration where the blue dot and black arrow is the evader and its velocity orientation, the large blue circle is the evader's sensing region; and (b)–(d) the trajectories of the pursuer (red line) and evader (blue line) until capture is achieved.

Table 1. Parameter values for the pursuer and evader for simulations.

Parameter	Symbol	Value
Pursuer speed	V_P	1.05 m s^{-1}
Pursuer steering gain	K_P	50 rad s^{-1}
Pursuer appendage length	l_f	316×10^{-3} m
Pursuer body length	l_P	378×10^{-3} m
Pursuer body width	w_P	44.8×10^{-3} m
Evader sensing range	R	1.0 m
Evader steering gain	K_E	50 rad s^{-1}
Evader speed	V_E	1.0 m s^{-1}
Evader burst duration	β	0.25 s
Evader coast duration	$\mathcal{T}$	2.75 s
Environment bounds	$\mathcal{B}$	$\{\mathcal{B} \in \mathbb{R}^2 \mid \lvert x \rvert \leqslant 1.5\ \mathrm{m}, \lvert y \rvert \leqslant 1.5\ \mathrm{m}\}$

concept of an avoidance region $\mathcal{A} \subset \mathcal{R}_{\mathcal{S}}$, defined as any intersection of the sensing region and the boundary and any intersection of the sensing region and the pursuer. Let there be a single avoidance region per set of intersections such that there are $N \geqslant 0$ avoidance regions in total. Let $\phi_{\mathcal{A}}(\psi)$ be a matrix containing each set of avoided directions, where

$$\phi_{\mathcal{A}}(\psi) = \begin{bmatrix} \theta_{AL}(\psi) & , & \theta_{AR}(\psi) \\ \theta_{\mathcal{B}_1} & , & \theta_{\mathcal{B}_2} \\ & \vdots & \\ \theta_{\mathcal{B}_N} & , & \theta_{\mathcal{B}_{N+1}} \end{bmatrix} = \begin{bmatrix} \phi_{\mathcal{A}_1} & , & \phi_{\mathcal{A}_2} \\ \phi_{\mathcal{A}_3} & , & \phi_{\mathcal{A}_4} \\ & \vdots & \\ \phi_{\mathcal{A}_N} & , & \phi_{\mathcal{A}_{N+1}} \end{bmatrix}, \tag{23}$$

and let $\phi_{\mathcal{A}_n}$ and $\phi_{\mathcal{A}_{n+1}}$ be the intersection angles for the nth avoidance region.

We define the evader's escape region $\mathcal{E} \subset \mathcal{R}_{\mathcal{S}}$ as the compliment of $\mathcal{A}$, as shown in figure 6; let there be $M \geqslant 1$ escape regions. Let $\phi_{\mathcal{E}}(\psi)$ be a matrix containing each set of escape directions where

$$\phi_{\mathcal{E}}(\psi) = \begin{bmatrix} \phi_{\mathcal{A}_2} & , & \phi_{\mathcal{A}_3} \\ \phi_{\mathcal{A}_4} & , & \phi_{\mathcal{A}_5} \\ & \vdots & \\ \phi_{\mathcal{A}_{N+1}} & , & \phi_{\mathcal{A}_1} \end{bmatrix} = \begin{bmatrix} \phi_{\mathcal{E}_1} & , & \phi_{\mathcal{E}_2} \\ \phi_{\mathcal{E}_3} & , & \phi_{\mathcal{E}_4} \\ & \vdots & \\ \phi_{\mathcal{E}_M} & , & \phi_{\mathcal{E}_{M+1}} \end{bmatrix}, \tag{24}$$

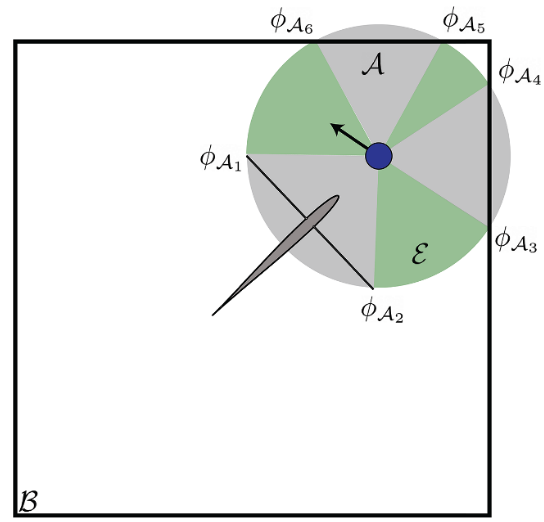

Figure 6. Illustration of the evaders sensing region divided into avoidance regions and escape regions. The gray avoidance regions are defined by the intersection angles between the sensing region, the pursuer's appendages, and the boundary (black lines). The green escape regions are the spaces where the evader's possible escape routes exist.

and let $\phi_{\mathcal{E}_m}$ and $\phi_{\mathcal{E}_{m+1}}$ be the intersection angles for the mth escape region. The size of the mth escape region is

$$\delta_{\mathcal{E}_m}(\psi) = \begin{cases} R\left(2\pi - \arg\left(e^{j\left(\phi_{\mathcal{E}_m} - \theta_{\mathcal{E}_{m+1}}\right)}\right)\right), \\ \qquad \text{ccw arc length} > \pi \\ R\left(\arg\left(e^{j\left(\phi_{\mathcal{E}_m} - \theta_{\mathcal{E}_{m+1}}\right)}\right)\right), \\ \qquad \text{otherwise.} \end{cases} \tag{25}$$

Note that $\delta_{\mathcal{E}_m}$ and $\boldsymbol{\phi}_{\mathcal{E}}$ are also implicitly dependent on the relative distance between the pursuer and evader.

If there are $N = 0$ avoidance regions, then $\boldsymbol{\phi}_{\mathcal{A}}$ is a null matrix and there are $M = 1$ escape regions, where $\boldsymbol{\phi}_{\mathcal{E}} = [0, 2\pi]$. When there are $N \geqslant 1$ avoidance regions, there are $M = N$ escape regions. We use (24) and (25) to compute the probability density function for the evader's protean strategy and to compute the expected work required for the pursuer to capture the evader in section 4.

3.3. Probability density function of the evader's heading

This section defines the evader's probability density function for the random escape heading θ_d. During the active steering phase, the evader steers to θ_d to avoid capture from the pursuer and to avoid collisions with the boundary. The probability density function for θ_d is dependent on the number of escape regions M and the arc length of each individual escape region $\delta_{\mathcal{E}_m}$.

When there are $N = 0$ avoidance regions and $M = 1$ escape regions, the evader chooses θ_d with a uniform probability density such that $0 \leqslant \theta_d \leqslant 2\pi$. The corresponding probability density function for the $N = 0$ case is

$$f(\theta_d) = \begin{cases} \frac{1}{2\pi}, & 0 \leqslant \theta_d \leqslant 2\pi \\ 0, & \text{otherwise} \end{cases}. \tag{26}$$

For the general $N = M \geqslant 1$ case, let $\phi_{\mathcal{E}_n}$ and $\phi_{\mathcal{E}_{n+1}}$ be the pair of headings for the nth escape region and let $\delta_{\mathcal{E}_n}$ be the corresponding arc length. The probability density function for θ_d is

$$f(\theta_d) = \begin{cases} \frac{\delta_{\mathcal{E}_1}}{\sum_{m=1}^{N} \delta_{\mathcal{E}_m}^2}, & \phi_{\mathcal{E}_2} - \delta_{\mathcal{E}_1}/R < \theta_d < \phi_{\mathcal{E}_2} \\ \vdots & \\ \frac{\delta_{\mathcal{E}_N}}{\sum_{m=1}^{N} \delta_{\mathcal{E}_m}^2}, & \phi_{\mathcal{E}_{N+1}} - \delta_{\mathcal{E}_N}/R < \theta_d < \phi_{\mathcal{E}_{N+1}} \\ 0, & \text{otherwise} \end{cases}. \tag{27}$$

Figure 7 illustrates the evader's probability density function for θ_d. The positions of the pursuer and evader are shown in figure 7(a), where the evader is also near two boundaries. The corresponding probability density function θ_d is computed using (27) and is shown in figure 7(b).

In the next section, we use (27) to compute the expected work to capture the evader for the resting appendages case, $\psi = 0$, and for the active appendages case, $\psi = \pi/2$. We can determine when it is advantageous for the pursuer to expand its appendages by comparing the expected work for these two cases.

4. Shape-changing predation strategy

This section analyzes the use of the pursuer's appendages to aid in capturing the evader. First, we compute the work required for the pursuer to capture the evader as a function of the appendage orientation ψ. Second, we derive the expected work to capture the evader using the evader's probability density function for its escape heading. Third, we compare the expected work for the $\psi = 0$ and $\psi = \pi/2$ cases to determine when the efforts to trap the evader outweighs the additional effort due to increased drag.

4.1. Work to capture the evader and the expected work

Since the pursuer has a constant speed V_P, its thrust and drag forces are balanced, i.e. $T_P = D_p$, and T_P is aligned with the pursuer's velocity V_P. Substituting (13) into (9) gives the work required to capture the evader during its non-active steering phase, i.e.

$$W_P(\psi) = b\left(1 + H\sin(\psi)\right) V_P |r_{E/P_f}| \times \left(\frac{K^2 + K\cos(\alpha - \theta_e)}{K^2 - 1}\right). \tag{28}$$

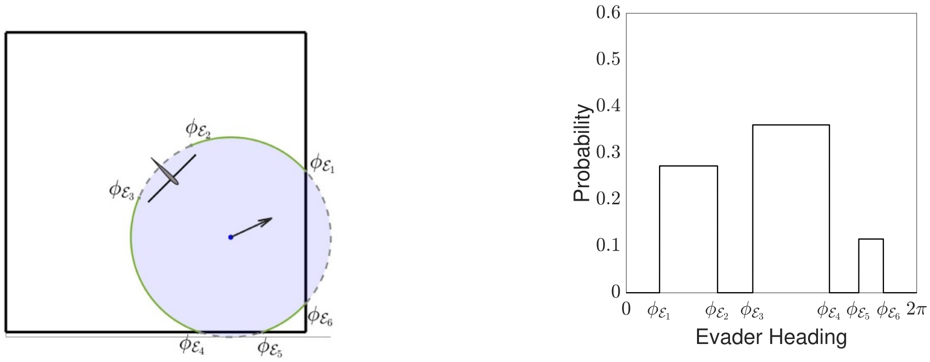

(a) Pursuer evader configuration

(b) Probability density function of the evader's escape direction

Figure 7. Probability density function of the evader's escape direction as a function of the relative position with the pursuer and proximity to the boundary (black lines). (a) The pursuer and the boundary are in the evader's blue sensing region, the solid green lines represent the evader's possible escape directions, and the dashed gray lines represent the evader's avoidance directions; (b) the corresponding probability density function for the evader's escape heading.

The work to capture the evader depends on the evader's heading θ_e and the pursuer's appendage orientation ψ. Regardless of the evader's heading, the work for $\psi = 0$ is always less than the work for $\psi = \pi/2$ for all $H > 0$, where H is the drag increase due to appendage expansion. Computing the work alone does not account for the minimization of the evader's escape routes by expanding the appendages, so instead we use the expected work.

Due to the stochastic nature of the evader's heading, we compute the expected value of work by substituting (28) into (4) and evaluate the integral with the appropriate probability density function for the evader's heading.

For the $N = 0$ case, neither the pursuer nor the boundary are in the sensing region and the evader's escape heading probability density function is (26). The corresponding expected work is

$$E[W_P(\psi)] = \frac{b\,(1 + H\sin(\psi))\,V_P|r_{E/P_f}|}{K^2 - 1}K^2. \tag{29}$$

Since the pursuer is beyond the sensing region, (29) does not depend on the minimization of escape routes, and the expected work for $\psi = 0$ is always less than the expected work for $\psi = \pi/2$, i.e. $E[W_p(\psi = 0)] < E[W_P(\psi = \pi/2)]$ for $N = 0$. Therefore, when there are no avoidance regions and when $|r_{E/P_f}| > R$ it is never advantageous for the pursuer to expand the appendages.

For the general $N \geqslant 1$ case, the probability density function for the evader's escape heading is (27) and the expected work is

$$E[W_P(\psi)] = \frac{b\,(1 + H\sin(\psi))\,V_P|r_{E/P_f}|}{(K^2 - 1)\sum_{m=1}^{N}\delta^2_{\mathcal{E}_m}(\psi)}X(\psi), \tag{30}$$

where

$$X(\psi) = \sum_{q=1}^{N}\delta_{\mathcal{E}_q}(\psi)\left(K^2\frac{\delta_{\mathcal{E}_q}(\psi)}{R} + K\left(\sin(\alpha - \phi_{\mathcal{E}_{2q}}) - \sin\left(\alpha - \phi_{\mathcal{E}_{2q}} - \frac{\delta_{\mathcal{E}_q}(\psi)}{R}\right)\right)\right). \tag{31}$$

Unlike the actual work in (28), the expected work in (30) accounts for the reduction in the evader's escape region due to the boundary and the orientation of the pursuer's appendages.

4.2. Minimizing the expected work

This section uses the expected work in (30) to analyze the trade-off between minimizing the evader's escape region and minimizing the work to capture. In general, the advantages from expanding the appendages depends on the additional drag H felt by the pursuer. To analyze this trade-off we evaluate the conditions on H that satisfy

$$E[W_P(\psi = \pi/2)] \quad \leqslant \quad E[W_P(\psi = 0)]. \tag{32}$$

Condition (32) is called the shape-changing condition and is satisfied if the expected work to capture the evader with expanded appendages is less than or equal to the expected work with swept back appendages.

Substituting (30) into (32) yields the following condition on H:

$$H \leqslant \left(\frac{X(0)}{X(\pi/2)}\sum_{m=1}^{N}\frac{\delta^2_{\mathcal{E}_m}(\pi/2)}{\delta^2_{\mathcal{E}_m}(0)}\right) - 1. \tag{33}$$

Condition (33) is called the max drag increase condition and acts as an upper limit to the amount of additional drag due to appendage expansion when condition (32) is also satisfied.

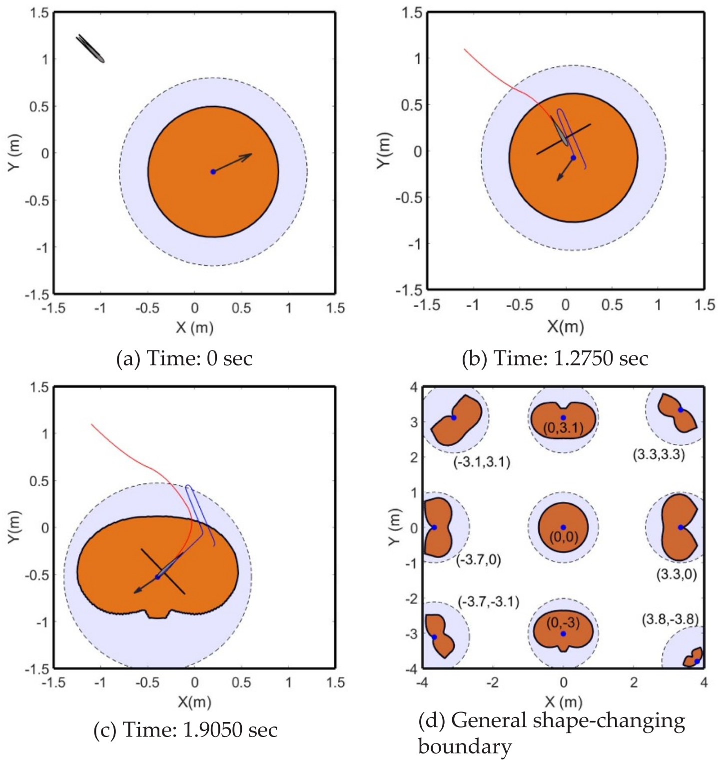

Figure 8. Numerical illustrations of the shape-changing boundary (orange region) during pursuit with a 15% increase in drag due to appendage expansion: (a) the evader (blue dot) is far from the boundary so the shape-changing boundary has axial symmetry; (b) the pursuer enters the evader's sensing region (blue circle) and the shape-changing boundary so it expands it appendages to minimize the evader's escape directions; (c) the evader is near the domain boundary so the shape-changing boundary loses axial symmetry and the evader is also captured; (d) the shape-changing boundary for a variety of evader positions in the bounded environment.

During pursuit, if the pursuer's additional drag $H > 0$ satisfies the condition in (33), then the minimization of the evader's escape region outweighs the minimization of the pursuer's work to capture, and the pursuer should expand its appendages. For practical systems, the exact value of H depends on the geometry of the pursuer's body.

The remainder of this paper discusses how conditions (32) and (33) affect the predation strategy of the pursuer.

4.3. The optimal shape-changing boundary

This section numerically analyzes the spaces where conditions (32) and (33) are satisfied in the bounded environment. To illustrate the spaces where it is advantageous for the pursuer to extend the appendages, we place the evader in a fixed location and evaluate condition (32) for varying positions of the pursuere additional drag was assumed t. The boundary of the area under which conditions (32) and (33) are satisfied is called the shape-changing boundary. During pursuit, if the pursuer crosses the shape-changing boundary, then it should extend its appendages to minimize the evader's escape directions; otherwise, it should relax its appendages to minimize drag. The geometry of the shape-changing boundary depends on the evader's proximity to the walls of the domain and the geometrical changes in the shape-changing boundary gives insights to the role of environment in the pursuit-evasion interaction.

In figures 8(a)–(c), we numerically compute the shape-changing boundary for the predation trajectories shown in figure 5 with the additional drag set to $H = 0.15$. When the evader is far from the walls of the environment, the shape-changing boundary has axial symmetry with a radius less than the evader's max sensing range, see figures 8(a) and (b). Due to the evader's inability to respond when the pursuer is beyond the sensing range, the radius of the shape-changing boundary is always less than or equal to the sensing radius. When the evader is near the walls of the environment, the shape-changing boundary loses axial symmetry and its geometry depends on the its proximity to one or multiple walls; see figure 8(c).

Figure 8(d) shows the shape-changing boundary for multiple evader positions with $H = 0.15$ and $R = 1$. When the evader is near a single wall, the shape-changing boundary's maximum radial distance is parallel to the wall and the minimal radial distance is perpendicular to the wall. The maximal radial distances implies that the pursuer can minimize its expected work earlier in the interaction, whereas, the minimal radial distances implies that the pursuer needs to get closer to the evader before it can expand its appendages. As the evader approaches a single wall, the area of the shape-changing boundary

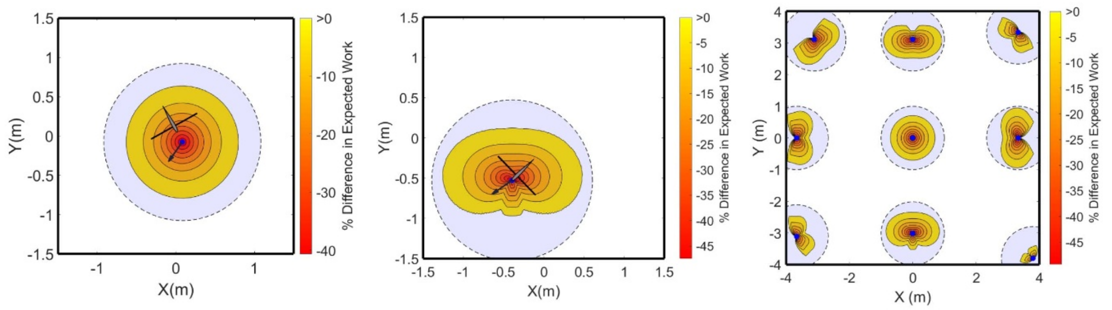

(a) Time: 1.2750 sec (b) Time: 1.9050 sec (c) Multiple evader locations

Figure 9. Numerically computed level curves for the percent difference in expected work to capture the evader during pursuit and a 15% increase in drag: (a) the evader is far from the domain boundaries and the level curves of the percent difference in expected work have axial symmetry; (b) the evader is near a single wall with optimal pursuit trajectories being approximately parallel to the boundary minimizing the number of the evader's escape regions; (c) the percent difference level curves for variety of evader locations.

decreases and it becomes increasingly less advantageous to approach the evader in directions perpendicular to the wall. Similar trends are observed, when the evader is near multiple walls.

Since the geometry of the shape-changing boundary changes with the evader's proximity to the environmental boundaries, the walls can be used to aid the pursuer by providing optimal pursuit trajectories that minimize the expected work earlier in the interaction. Notice that the area of shape-changing boundary greatly decreases when the evader is close to the corner of the closed environment; see lower right corner of figure 8(d). The large decrease in area implies that while there are optimal pursuit trajectories, the distance between the pursuer and evader needs to be small before the shape-changing condition is valid. Further implications of this scenario suggest that as the evader gets more cornered by the environment, it becomes less advantageous to trap the evader with the appendages. Also, notice that the shape-changing boundary exists even when the evader is far from walls. This implies that there are advantages to using the appendages to trap the prey even in perceived open spaces. Optimal pursuit trajectories become more evident when evaluating the level curves of the percent difference in expected work.

While figure 8 illustrates the outer limits of the shape-changing boundary, the figures in figure 9 illustrate the level curves of the percent difference in the expected work to capture the evader due to extending the appendages. The percent difference in expected work is computed by evaluating $E[W_P(\pi/2)]$ and $E[W_P(0)]$, from (30), for a fixed evader location and all possible pursuer locations, and using the following formula:

$$\%\mathrm{Diff} = 100\left(\frac{E[W_P(\pi/2)] - E[W_P(0)]}{E[W_P(0)]}\right). \quad (34)$$

Following the gradient of the percent difference level curves yields an optimal pursuit trajectory.

In cases where the evader is far from boundaries, see figure 9(a), the level curves maintain axial symmetry with increasing reductions in expected work as $|r_{E/P_f}|$ decreases. The axial symmetry of the level curves implies that there are no sub-optimal pursuit trajectories when the evader is far from boundaries. Optimal pursuit trajectories appear when the evader is near a boundary. Figures 9(b) and (c) show the level curves of the percent difference when the evader is near a single wall and the level curves for a variety of evader positions respectively. When near a single wall, the sub-optimal trajectories are perpendicular to the detected boundary and the optimal trajectories are parallel to the boundary. When the evader is near a detected boundary, the optimal pursuit trajectories imply that directly cornering the evader such that it has an equal probability of choosing any escape direction parallel with the boundary is sub-optimal. In cases when the evader is near a single wall or near a corner, the optimal pursuit trajectories minimize the number of escape regions for the evader. This qualitative analysis suggests that the optimal pursuit trajectories seek to eliminate the evader's split unpredictable flee directions making the evader's behavior more predicable.

Thus far, the additional drag was assumed to be $H = 0.15$; however, the max allowable additional drag is computed with (33). To illustrate how the additional drag affects the shape-changing boundary, we evaluate (33) for a fixed evader position and all possible pursuer positions in the bounded environment. Figures 10(a) and (b) show snapshots during pursuit with the level curves of the maximum additional drag that satisfies (32). The level curve of the additional drag for $H = 0.15$ is equivalent to the outer limit of the shape-changing boundary in figure 8. In general, as the value of H increases the radius of the shape-changing boundary decreases; see figure 10(c). For

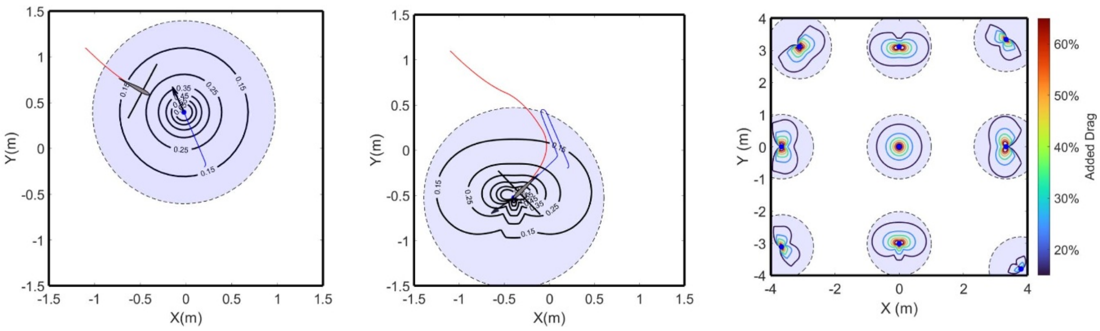

(a) Time: 0.6350 sec (b) Time: 1.9050 sec (c) Multiple evader locations

Figure 10. Snapshots of the pursuit trajectories with numerical illustrations of the shape-changing boundary for various drag coefficients: (a) as the pursuer approaches the evader and crosses the shape-changing boundary for $H = 0.15$ it expands its appendages to minimize the evader's escape directions; (b) the evader is captured near a detectable wall and the level curves of the shape-changing boundary loses axial symmetry; (c) the level curves of the added drag for multiple evader positions.

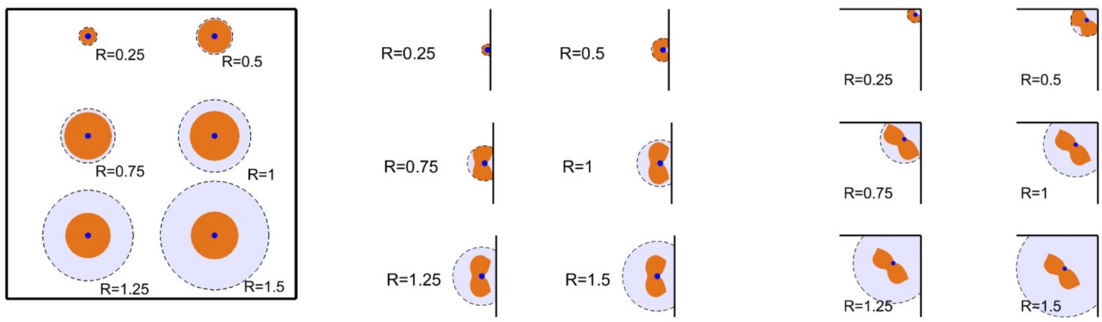

(a) Far from walls (b) Near a single wall (c) Near a corner

Figure 11. Numerical illustrations of the the shape-changing boundary for various sizes of the evader's sensing region and various evader positions in a bounded environment: (a) the evader is placed at six positions in the environment where it does not sense the walls and shape-changing boundary maintains axial symmetry; (b) the evader is near a single wall and the 20% of the sensing region is excluded by the boundary; (c) the evader is in the corner of the environment and 20% of the sensing region is excluded by the boundary.

higher values of H, the pursuer needs to get closer to the evader before it is advantageous to minimize the evader's escape directions. While there are benefits for this predation strategy for high values of additional drag, the close proximity requirement makes it less tractable.

Due to the assumption that the evader is unresponsive until the pursuer or boundary are in the sensing region, the size of the evader's sensing region effects the interaction. Figures 11(a)–(c) illustrate how the radius of the sensing region effects the shape changing boundary for various evader interactions with the walls. Depending on the evader's position in the environment, the sensing radius scales and truncates the shape-changing boundary.

In figure 11(a) the evader is placed in six locations far from the walls in the environment and the shape-changing boundary maintains axial symmetry regardless of sensing radius. For small sensing radii, the radial distance of the shape-changing boundary decreases. As the sensing radius increase, the size of the shape-changing boundary increases until it reaches an upper limit. Similar trends are followed when the evader is near a single wall in figure 11(b) and when the evader is near a corner in figure 11(c). For consistency, the evader is positioned such that 20% of its sensing region is blocked by the environmental boundary for each sensing radii in figures 11(b) and (c). A small sensing radius in conjunction with close proximity to a wall truncates the shape-changing boundary and decreases its scale; however, as the sensing region increases, the scaling and truncation diminishes and the area of the shape-changing boundary approaches a constant. Overall, the shape and geometry of the shape-changing boundary is determined by evader's position and proximity to the walls of the environment and the scale and truncation of the shape-changing

Figure 12. Lionfish (*Pterois volitans*) with its pectoral fins flared.

boundary is determined by the evader's sensing radius. The shape-changing boundary's convergence to a constant maximum area is due to the trade-off of the shape-changing strategy. The pursuer's appendages are less effective at blocking the evader's field of view at greater distances, so the pursuer should prioritize minimizing drag until it reaches the shape-changing boundary.

5. Conclusion

This paper presents a bioinspired pursuit-evasion game in a closed environment with one pursuer and one evader. We model the pursuer as a streamlined body with symmetrically actuated appendages in pure pursuit of an intermittently steering point mass evader. To avoid capture, the evader uses a protean strategy, which steers in a random escape direction to be less predictable to the pursuer. The evader's random escape direction has a probability density function that depends on its proximity to the pursuer, the boundary, and the orientation of the pursuer's appendages. This bioinspired shape-changing predation strategy allows the pursuer to actively use its appendages to trap the evader by minimizing the evader's escape routes, but at the cost of incurring additional hydrodynamic drag. Ultimately, this work investigates the trade-off between minimizing the work to capture the evader and using appendages to trap the evader. We show that actively using the appendages to trap the evader outweighs the effects of additional drag once the pursuer is sufficiently close to the evader. Furthermore, we show that the environments boundaries can be used to aid the pursuer by providing optimal pursuit trajectories that minimize the expected work to capture the evader and make the evader's flee direction more predictable.

During a pursuit-evasion interaction with a stochastic evader, the pursuer does not know the direction the evader will steer, the total duration of the interaction, or the total amount of work required to capture the evader. In an effort to reduce the variance of stochasticity during the interaction, the pursuer can employ the shape-changing strategy. Once the pursuer is in the evader's sensing region, the pursuer can expand its appendages to reduce the evader's possible flee directions, making the evader's next decision more predictable, albeit at the cost of incurring additional drag and increasing the momentary work. The shape-changing strategy is beneficial to the pursuer in both open and closed environments, but additional benefits exist for closed environments, or at least environments with structures. The walls of the environment act as obstacles for the evader and further reduce the variance of its flee direction. A pursuer can exploit these obstacles in conjunction with the shape-changing strategy to influence the evader. When the evader is near a single wall or corner, approaching it in certain directions can cause a bifurcation in the evader's flee direction. These bifurcations are less favorable to the pursuer because it splits the overall probability that the evader will choose either the left or right direction. Instead, the pursuer should take a trajectory that exploits the walls and forces the evader to swim in one general direction. As the evader gets closer to the boundary, the appendages become less useful and the pursuers should prioritize minimizing drag.

Drag has an integral role in the shape-changing strategy. The pursuer's nominal drag affects the magnitude the work and expected work to capture, but the added drag from appendage expansion makes the shape-changing strategy viable. If the added drag is above an upper limit, then using the appendages to reduce the evader's randomness never outweighs minimizing the work to capture. As the added drag decreases, the benefit of using the shape-changing strategy increases. For practical robotic systems, the design of the appendages can again draw inspiration from the lionfish (*Pterois volitans*), whose pectoral fins are comprised of several feather-like spines, see figure 12. A similar appendage structure would allow the robot to greatly increase its ability to block the evader's field of view while not significantly increasing its own hydrodynamic drag.

The evader's sensing radius also plays a role in the pursuit-evasion interaction. In open environments, the radius of the evader's sensing region is directly proportional to the scale of shape-changing boundary until the sensing radius is greater than the shape-changing boundary's max-radial distance. Near the walls of the environment the sensing radius and the wall contribute to the scaling and truncation of the shape-changing boundary. From the evader's point of view, a small sensing radius means that the evader cannot respond to the pursuer until it is maybe too late; whereas, a larger sensing radius means that the evader can respond sooner. As the sensing radius increases, the field of view blocked by the expanded appendages decreases when the pursuer enters the sensing region. This inverse proportional relationship implies that the pursuer's width and appendage length influence the scale of the shape-changing boundary and that optimizing these parameters yields the optimal size of the shape-changing boundary. Understanding the full effects of the evader's sensing radius over the entire interaction is a suitable topic for ongoing and future research.

Inspired by the characteristics of lionfish predation, the present work provides a mathematical model that investigates the trade-off between minimizing the work to capture and using drag-inducing appendages to trap an evader and implements a shape-changing strategy. We do not claim that the shape-changing strategy accurately models lionfish pursuit behavior, but it may be a viable pursuit tactic for a variety of engineered and robotic systems not limited to the underwater domain.

Ongoing and future work seeks to vary the size of the environment, the sensing radius, and the relative speeds of both agents for the shape-changing strategy and other pursuit strategies to measure its comparative performance. Other possible research directions to expand this work to include cases with a slower pursuer and an intermittently faster evader, multiple flocking evaders and a single pursuer, and the consideration of additional structures in the environment.

Data availability statement

All data that support the findings of this study are included within the article (and any supplementary files).

ORCID iDs

Anthony A Thompson https://orcid.org/0000-0001-5231-5213
Matthew J McHenry https://orcid.org/0000-0001-5834-674X

References

[1] Albins M A and Lyons P J 2012 *Mar. Ecol. Prog. Ser.* **448** 1–5
[2] Albins M A and Hixon M A 2013 *Environ. Biol. Fishes* **96** 1151–7
[3] Green S J, Akins J L and Côté I M 2011 *Mar. Ecol. Prog. Ser.* **433** 159–67
[4] Soto A P and McHenry M J 2020 *J. Exp. Biol.* **223** jeb230623
[5] Peterson A N 2022 The persistent-pursuit and evasion strategies of lionfish and their prey *PhD Thesis* UC Irvine
[6] Peterson A N and McHenry M J 2022 *Proc. R. Soc.* B **289** 20221085
[7] Tornabene L and Baldwin C C 2017 *PLoS One* **12** e0177179
[8] Côté I M and Maljković A 2010 *Mar. Ecol. Prog. Ser.* **404** 219–25
[9] McHenry M J, Johansen J L, Soto A P, Free B A, Paley D A and Liao J C 2019 *Proc. R. Soc.* B **286** 20182934
[10] Peterson A N, Soto A P and McHenry M J 2021 *Integr. Comp. Biol.* **61** 668–80
[11] Humphries D and Driver P 1970 *Oecologia* **5** 285–302
[12] Nair A, Changsing K, Stewart W J and McHenry M J 2017 *Proc. R. Soc.* B **284** 20170393
[13] Soto A, Stewart W J and McHenry M J 2015 *Integr. Comp. Biol.* **55** 110–20
[14] Shneydor N A 1998 *Missile Guidance and Pursuit: Kinematics, Dynamics and Control* (Amsterdam: Elsevier) pp 51–55
[15] Isaacs R 1999 *Differential Games: A Mathematical Theory With Applications to Warfare and Pursuit, Control and Optimization* (New York: Courier Corporation)
[16] Fuchs Z E, Khargonekar P P and Evers J 2010 Cooperative defense within a single-pursuer, two-evader pursuit evasion differential game *49th IEEE Conf. on Decision and Control* pp 3091–7
[17] Scott W and Leonard N E 2014 Dynamics of pursuit and evasion in a heterogeneous herd *53rd IEEE Conf. on Decision and Control* pp 2920–5
[18] Pan S *et al* 2012 Pursuit, evasion and defense in the plane *2012 American Control Conf.* pp 4167–73
[19] Bakolas E and Tsiotras P 2010 Optimal pursuit of moving targets using dynamic Voronoi diagrams *49th IEEE Conf. on Decision and Control* pp 7431–6
[20] Dorothy M, Maity D, Shishika D and Von Moll A 2021 arXiv:2111.09205
[21] Free B A, McHenry M J and Paley D A 2019 *J. R. Soc. Interface* **16** 20180873
[22] Free B A, Lee J and Paley D A 2020 *Bioinspir. Biomim.* **15** 035005
[23] Jin S and Qu Z 2010 Pursuit-evasion games with multi-pursuer vs. one fast evader *2010 8th World Congress on Intelligent Control and Automation* pp 3184–9
[24] Ramana M and Kothari M 2015 A cooperative pursuit-evasion game of a high speed evader *2015 54th IEEE Conf. on Decision and Control* pp 2969–74
[25] Ydenberg R C and Dill L M 1986 The economics of fleeing from predators *Advances in the Study of Behavior* vol 16 (Amsterdam: Elsevier) pp 229–49
[26] Burghart E, Mar M, Rivera S G, Zepecki C and Blumstein D T 2023 *J. Exp. Mar. Biol. Ecol.* **561** 151871
[27] Ramana M V and Kothari M 2017 *J. Intell. Robot. Syst.* **85** 293–306
[28] Weihs D and Webb P W 1984 *J. Theor. Biol.* **106** 189–206
[29] Moore T Y, Cooper K L, Biewener A A and Vasudevan R 2017 *Nat. Commun.* **8** 1–9
[30] Kramer D L and McLaughlin R L 2001 *Am. Zool.* **41** 137–53
[31] Bazazi S, Bartumeus F, Hale J J and Couzin I D 2012 *PLoS Comput. Biol.* **8** e1002498
[32] Lunsford E T, Skandalis D A and Liao J C 2019 *J. Neurophysiol.* **122** 2438–48
[33] Hahn L S 1994 *Complex Numbers and Geometry* vol 1 (Cambridge: Cambridge University Press) pp 24–25

[34] Brown R G and Hwang P Y 1997 *Introduction to Random Signals and Applied Kalman Filtering: With MATLAB Exercises and Solutions* (New York: Wiley) pp 214–20
[35] Kasdin N J and Paley D A 2011 *Engineering Dynamics* (Princeton, NJ: Princeton University Press) pp 148–50
[36] Thompson A A, Cañuelas L and Paley D A 2022 Estimation and control for collective motion with intermittent locomotion *2022 American Control Conf.* pp 747–54
[37] Ruiz-Carus R, Matheson R E Jr, Roberts D E Jr and Whitfield P E 2006 *Biol. Conserv.* **128** 384–90